

Finite element analysis of magnesium AZ80 wrought alloy anisotropic behaviour during warm forging

D. Kobold*, G. Gantar**, T. Pepelnjak***

*TECOS Slovenian Tool and Die Development Centre, Kidričeva 25, SI-3000 Celje, Slovenia,

E-mail: dominik.kobold@tecos.si

**Envita, Tržaška 132, SI-1000 Ljubljana, Slovenia, E-mail: gasper.gantar@envita.si

***Faculty of Mechanical Engineering University of Ljubljana, Aškerčeva 6, SI-1000 Ljubljana, Slovenia,

E-mail: tomaz.pepelnjak@fs.uni-lj.si

crossref <http://dx.doi.org/10.5755/j01.mech.18.3.1876>

1. Introduction

Numerical simulations has become a widely used tool in forging shops due to their significant advantages in optimization and tailored design of the forging process in terms of proper die cavities and slug design as well as in the determination of (multiple) forging operations without inefficient trial-error-repair efforts [1, 2].

This paper deals with FEM simulations of bulk forming (forging) of magnesium wrought alloy AZ80 in warm conditions.

Magnesium and its alloys are characterised by significant anisotropic properties mainly influenced by hexagonal close-packed (h.c.p.) basal crystal cells and the pre-deformation process (pre-extrusion, rolling, etc.) applied during preparation process of magnesium wrought alloys [3-5]. However, the pre-deformation process is essential for reduction of grain sizes, but causes formation of texture with strong grain orientation in the extrusion direction [3-5]. Furthermore, formation of sliding planes (prismatic and pyramidal) and twinning mechanisms in h.c.p. is significantly dependent on loading (deformation) direction as well as on temperature, since sufficient plastic deformation in conventional forming processes is possible only at temperatures above 230°C [3-5].

Most FEM computations in bulk metal forming use a phenomenological model of plasticity in which the metal is treated as an isotropic body. However, the anisotropic behaviour of magnesium pre-extruded alloys has been recognised as a major phenomenon affecting material flow during applied plastic deformation [3, 5]; therefore, consideration of anisotropic behaviour is crucial in FEM modelling of the bulk forming process of Mg alloys. It is also a major challenge to incorporate the initial plastic anisotropy of the metal into the phenomenological model of plasticity and to describe subsequent plastic deformation [6].

The modelling of anisotropic behaviour and the material flow of h.c.p. polycrystalline materials during the applied plastic deformation using FEM simulations require consideration of highly complicated equations incorporating both single crystal responses and associated interaction laws describing texture changes [4, 6]. Unfortunately such FEM simulations are extremely time consuming; moreover, they are still not applicable for industrial practice but are used only for simulating deformation of very small areas or single crystals [4, 6]. For industrial practice, classic formulations for anisotropic behaviour of cubic metals

such is Hill's (1948) quadratic anisotropic yield law [7] are still used in FEM models [4-6, 8] due to a lack of adequate macroscopic criteria for h.c.p. materials.

In this paper, a simplified approach for the determination of the anisotropic properties of magnesium AZ80 alloy during deformation is used. Anisotropic properties were defined by Hill's anisotropic coefficients F , G , H , L , M and N , which are determined as constants throughout the plastic deformation. Despite all of this, these simplifications enable defining robust FEM models applicable for industrial practice, which enable reliable computations of anisotropic material flow in a reasonable time.

Hill's anisotropic coefficients were determined for the case of pre-extruded magnesium AZ80 alloy on the basis of previous experimentally obtained main yield and shear yield stresses (mechanical properties) for general use in a form of flow curves [9] and on the basis of a study for the determination of anisotropic material flow under a wide range of different process parameters [5].

Furthermore, an extensive FEM study of upsetting and radial compressing of small cylindrical specimens as well as forging of complex industrial-scale parts were performed using Deform 3D V10 software code.

Additionally, to evaluate the accuracy of the FEM results, a comparison between 3D-digitised shapes of real forged specimens (parts) and FEM computed 3D-shapes was performed.

This paper directly contributes to the usage of FEM simulations in industrial practice, because very promising results have been obtained for anisotropic materials on the basis of defined robust FEM models. With the use of FEM simulations, producing of tailored net-shape faultless parts can be achieved efficiently.

2. Constitutive equations of Hill's (1948) quadratic anisotropic yield law

In 1948, Hill proposed a quadratic anisotropic yield law for materials that are supposed to have anisotropy in the three orthogonal directions [7]

$$2f(\sigma_{ij}) = F(\sigma_{yy} - \sigma_{zz})^2 + G(\sigma_{zz} - \sigma_{xx})^2 + H(\sigma_{xx} - \sigma_{yy})^2 + 2L\tau_{yz}^2 + 2M\tau_{xz}^2 + 2N\tau_{xy}^2 \quad (1)$$

In Eq. (1), there are six independent anisotropic coefficients in which F , G , H are anisotropic coefficients of the main yield stresses and L , M , N are anisotropic coef-

ficients of the shear yield stresses in the principal axes of anisotropy.

Hill's anisotropic coefficients are obtained as functions of the main yield stresses

$$\left. \begin{aligned} 2F &= \frac{1}{Y^2} + \frac{1}{Z^2} - \frac{1}{X^2} \\ 2G &= \frac{1}{Z^2} + \frac{1}{X^2} - \frac{1}{Y^2} \\ 2H &= \frac{1}{X^2} + \frac{1}{Y^2} - \frac{1}{Z^2} \end{aligned} \right\} \quad (2)$$

and as functions of the shear yield stresses

$$2L = \frac{1}{R^2}, \quad 2M = \frac{1}{S^2}, \quad 2N = \frac{1}{T^2} \quad (3)$$

In order to give a complete description of material anisotropy, all three main yield stresses X , Y , Z and shear yield stresses R , S , T should be known according to the orientation of the principal axes of anisotropy.

In this study, a magnesium pre-extruded feedstock bar of AZ80 alloy was used. The pre-extruded bar represents an orthotropic body having rotational symmetry (cylindrical orthotropy) of mechanical properties.

Furthermore, in orthotropic bodies, material properties can be effectively described by denoting the orthogonal Cartesian coordinate system (Fig. 1) in which each coordinate axis designates the principal loading direction. In the case of a pre-extruded bar, the z axis represents longitudinal direction (LD) while the x and y axes are perpendicular to the z axis and at the same time mutually independent and equivalent, due to cylindrical orthotropy; therefore, it can be said that both represent the transverse direction (TD) [10].

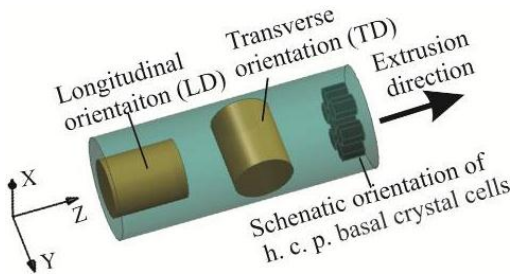


Fig. 1 Orientation of specimens

The bases for the determination of Hill's anisotropic coefficients were stress states (main yield and main shear yield stresses) in x , y and z orthotropic direction during deformation according to the loading conditions and process parameters; therefore, in each principal orthotropic direction, main yield stresses σ_{11} , σ_{22} , σ_{33} as well as shear yield stresses σ_{12} , σ_{23} , σ_{31} were identified.

Furthermore, it can be presumed that $\sigma_{11} = Z$, $\sigma_{22} = Y$, $\sigma_{33} = X$, $\sigma_{23} = R$, $\sigma_{12} = S$, $\sigma_{13} = T$. Eqs. (2) and (3) can be also expressed as follows [8].

Hill's anisotropic coefficients in Eq. (4) have MPa^{-2} units. However, Hill's anisotropic coefficients are usually given as dimensionless constants and when $F = G = H = 1$ and $L = M = N = 3$ correspond to von Mises yield criterion for isotropic materials [7, 8].

$$\left. \begin{aligned} F &= \frac{1}{2} \left(\frac{1}{(\sigma_{22})^2} + \frac{1}{(\sigma_{11})^2} - \frac{1}{(\sigma_{33})^2} \right) \\ G &= \frac{1}{2} \left(\frac{1}{(\sigma_{11})^2} + \frac{1}{(\sigma_{33})^2} - \frac{1}{(\sigma_{22})^2} \right) \\ H &= \frac{1}{2} \left(\frac{1}{(\sigma_{33})^2} + \frac{1}{(\sigma_{22})^2} - \frac{1}{(\sigma_{11})^2} \right) \\ L &= \frac{1}{2(\sigma_{23})^2}, \quad M = \frac{1}{2(\sigma_{12})^2}, \quad N = \frac{1}{2(\sigma_{13})^2} \end{aligned} \right\} \quad (4)$$

Finnie and Heller [8] primarily purposed formulations in Eq. (5) enabling calculations of Hill's dimensionless anisotropic coefficients.

$$\left. \begin{aligned} F &= \overline{\sigma_0}^{-2} \left(\frac{1}{(\sigma_{22})^2} + \frac{1}{(\sigma_{11})^2} - \frac{1}{(\sigma_{33})^2} \right) \\ G &= \overline{\sigma_0}^{-2} \left(\frac{1}{(\sigma_{11})^2} + \frac{1}{(\sigma_{33})^2} - \frac{1}{(\sigma_{22})^2} \right) \\ H &= \overline{\sigma_0}^{-2} \left(\frac{1}{(\sigma_{33})^2} + \frac{1}{(\sigma_{22})^2} - \frac{1}{(\sigma_{11})^2} \right) \\ L &= \frac{\overline{\sigma_0}^{-2}}{(\sigma_{23})^2}, \quad M = \frac{\overline{\sigma_0}^{-2}}{(\sigma_{13})^2}, \quad N = \frac{\overline{\sigma_0}^{-2}}{(\sigma_{12})^2} \end{aligned} \right\} \quad (5)$$

where $\overline{\sigma_0}$ [8, 11] can be expressed as

$$\overline{\sigma_0}^{-2} = 1/3 \left((\sigma_{11})^2 + (\sigma_{22})^2 + (\sigma_{33})^2 \right) \quad (6)$$

Because the initial anisotropic coefficients of Hill's (1948) quadratic anisotropic yield law in Deform 3D V10.0 software code are pre-set to $F = G = H = 0.5$ and $L = M = N = 1.5$ [12], the calculated values by formulations in Eq. (5) should be divided by the factor 2.

3. Previous experimental study background

Determination of Hill's anisotropic coefficients as constants was made: 1) on the basis of previously obtained main yield and shear yield stresses (mechanical properties) for general use in a form of flow curves [9] and 2) on the basis of lab-scale study for determining anisotropic material flow [5].

Main yield stresses were obtained with uniaxial upsetting while shear yield stresses were obtained with hat tests [9] in each nonequivalent orthotropic direction. Nonequivalent orthotropic loading direction was considered according to test specimens' orientation (LD and TD) regarding the extrusion direction of AZ80 feedstock bars in T5 condition as shown Fig. 1.

As previously stated, the main yield and shear yield stresses were obtained for general use in the form of flow curves at a wide range of process parameters: at initial temperatures of 250, 300, 350 and 400°C and constant strain rates $\dot{\phi}$ of 0.1, 1 and 10 s^{-1} according to the equiva-

lent strain φ from 0 to 1 [5, 9]. Data of the main yield and shear yield stresses were written as data arrays in which the value of the main yield or shear yield stresses at constant temperatures and strain rates have been given for each equivalent strain (φ) increment of 0.02 in range from $\varphi = 0$ to 1.

Flow curves representing the main yield stresses as a function of loading direction and strain rate at constant temperatures are illustrated in Fig. 2 [5, 9]. Major differences of the main yield stresses regarding the loading direction (Fig. 2, a) were observed. Main yield stresses in the LD direction are much bigger at the beginning of the plastic deformation to the strain of $\varphi \approx 0.4$ than in the TD direction. Moreover, significant deformation hardening/softening phenomenon during applied plastic deformation with major dependence on strain rates (see Fig. 2, b) is also observed. With increasing strain rates, the main yield stresses are growing and differences between the LD and TD directions are also increasing.

Main yield and shear yield stresses obtained at very high strain rates, i.e. $\dot{\varphi} = 10 \text{ s}^{-1}$, definitely enable very good definition of plastic characteristics during very fast deformation.

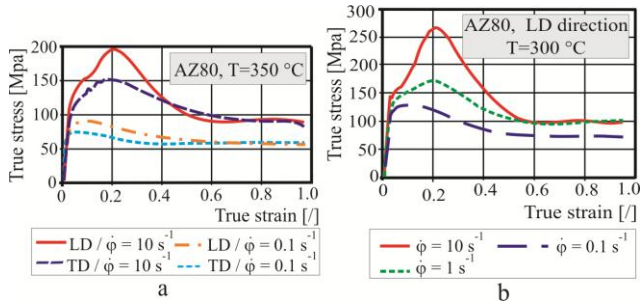


Fig. 2 Main yield stresses charts (flow curves) as a function of strain rate in a) LD and TD loading direction and b) in LD loading direction at constant temperature [5, 9]

Secondly, a lab-scale study for determining anisotropic material flow was performed using the same batch of the magnesium AZ80 pre-extruded feedstock bars as were used for obtaining the main yield and shear yield stresses [9]. In this study, cylindrical specimens with dimensions of $D_0 = 16 \text{ mm} \times L_0 = 20 \text{ mm}$ were machined from a pre-extruded AZ80 feedstock bar in the same orthotropic directions (LD and TD).

Specimens have been isothermally upset upright from start height of $L_0 = 20 \text{ mm}$ to end height of 6.7 mm as well as being isothermally compressed in radial position from a diameter of $D_0 = 16 \text{ mm}$ to an end height of 4 mm (Fig. 3) using different process parameters (initial temperature and ram speed). Initial temperatures were 300°C, 350°C and 400°C while upsetting and compressing was applied through constant ram speed (v) of 5 and 20 mm/s, respectively [5].

Differences in the final shapes of deformed specimens in the lab-scale study for determining anisotropic material flow are shown in Fig. 4 in Chapter 5.2.

4. Determination of Hill's anisotropic coefficients

4.1. Description of the determination of Hill's anisotropic coefficients for lab-scale study for determining anisotropic material flow

Hill's anisotropic coefficients were then determined as constants for each different variant of process parameters occurring during the lab-scale study for determining anisotropic material flow. For determination, Hill's anisotropic coefficients were used both for general-use-obtained main yield and shear yield stresses as well as results of the lab-scale study.

The most important result of the lab-scale study for determining anisotropic material flow were the final shapes of upset or compressed specimens. For deformed specimens, material extension in y and z orthotropic directions was measured, as shown in Fig. 3, while the third orthotropic direction x was always used as loading direction. With upset specimens D_T and D_L (see Fig. 3, a) and radial compressed specimens L_R (extension of material in radial direction) and L_F (extension of material in direction of flat planes), dimensions (Fig. 3, b) were measured according to each different input process parameter (initial specimen temperature, ram speed, specimen's placement and orientation). Due to the embossment of outer surfaces of deformed specimens, denoted dimensions in Fig. 3, a and b were measured between gravity centres of the embossed surface's arcs as shown Fig. 3, c.

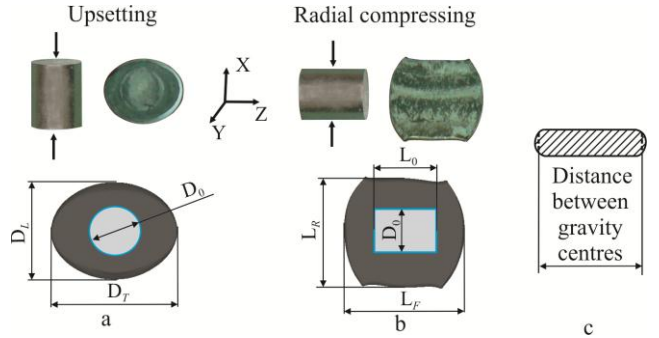


Fig. 3 Measured dimensions of a) upset and b) radial compressed specimens and c) measuring method

Afterwards, the above-denoted dimensions were used for calculation of logarithmic strains φ_{D_L} and φ_{D_T} at upsetting and φ_{L_R} and φ_{L_F} at radial compressing using the following equations

$$\varphi_{D_L} = \ln(D_L / D_0) \text{ and } \varphi_{D_T} = \ln(D_T / D_0) \quad (7)$$

$$\varphi_{D_L} = \ln(L_R / D_0) \text{ and } \varphi_{L_F} = \ln(L_F / L_0) \quad (8)$$

For each deformed specimen, average strain rates $\dot{\varphi}$ were then calculated using Eq. (9)

$$\dot{\varphi} = \frac{\ln(h_0 / h_1) v}{h_0 - h_1} \quad (9)$$

where h_0 is the initial height at which deformation was

began and h_1 the end height of deformed (upset or compressed) specimens through ram speeds v of 5 or 20 mm/s.

Table 1 shows all obtained values of the strains as consequence of material flow (extension) in y and z orthotropic directions during the deformation for each initial specimen's temperature, placement, orientation (LD and TD) and calculated average strain rate $\dot{\phi}$.

Table 1

Determined strains according to the different process parameters occurred in the lab-scale study for determining anisotropic material flow

Upsetting LD			
	300°C	350°C	400°C
$\dot{\phi} = 0.4 \text{ s}^{-1}$	$\varphi_{D_L} = 0.55$	$\varphi_{D_L} = 0.56$	$\varphi_{D_L} = 0.57$
	$\varphi_{D_T} = 0.55$	$\varphi_{D_T} = 0.56$	$\varphi_{D_T} = 0.57$
$\dot{\phi} = 1.6 \text{ s}^{-1}$	$\varphi_{D_L} = 0.55$	$\varphi_{D_L} = 0.56$	$\varphi_{D_L} = 0.58$
	$\varphi_{D_T} = 0.55$	$\varphi_{D_T} = 0.56$	$\varphi_{D_T} = 0.58$
Upsetting TD			
	300°C	350°C	400°C
$\dot{\phi} = 0.4 \text{ s}^{-1}$	$\varphi_{D_L} = 0.31$	$\varphi_{D_L} = 0.41$	$\varphi_{D_L} = 0.45$
	$\varphi_{D_T} = 0.75$	$\varphi_{D_L} = 0.71$	$\varphi_{D_L} = 0.67$
$\dot{\phi} = 1.6 \text{ s}^{-1}$	$\varphi_{D_L} = 0.31$	$\varphi_{D_L} = 0.41$	$\varphi_{D_L} = 0.43$
	$\varphi_{D_T} = 0.75$	$\varphi_{D_T} = 0.71$	$\varphi_{D_T} = 0.69$
Radial compressing TD			
	300°C	350°C	400°C
$\dot{\phi} = 0.6 \text{ s}^{-1}$	$\varphi_{L_R} = 0.65$	$\varphi_{L_R} = 0.67$	$\varphi_{L_R} = 0.75$
	$\varphi_{L_F} = 0.55$	$\varphi_{L_F} = 0.56$	$\varphi_{L_F} = 0.55$
$\dot{\phi} = 2.3 \text{ s}^{-1}$	$\varphi_{L_R} = 0.63$	$\varphi_{L_R} = 0.68$	$\varphi_{L_R} = 0.75$
	$\varphi_{L_F} = 0.57$	$\varphi_{L_F} = 0.57$	$\varphi_{L_F} = 0.55$
Radial compressing LD			
	300°C	350°C	400°C
$\dot{\phi} = 0.6 \text{ s}^{-1}$	$\varphi_{L_R} = 0.81$	$\varphi_{L_R} = 0.81$	$\varphi_{L_R} = 0.84$
	$\varphi_{L_F} = 0.42$	$\varphi_{L_F} = 0.47$	$\varphi_{L_F} = 0.45$
$\dot{\phi} = 2.3 \text{ s}^{-1}$	$\varphi_{L_R} = 0.81$	$\varphi_{L_R} = 0.84$	$\varphi_{L_R} = 0.88$
	$\varphi_{L_F} = 0.42$	$\varphi_{L_F} = 0.42$	$\varphi_{L_F} = 0.41$

Furthermore, for determining σ_{11} , σ_{22} , σ_{33} and σ_{12} , σ_{23} , σ_{13} were also used both for general-use-obtained main yield and shear stresses given as data arrays and logarithmic strains listed in the Table 1. The strains listed in Table 1 represent material flow in y and z orthotropic directions according to the all variants of process parameters occurring in the lab-scale study for determining anisotropic material flow. In the third orthotropic direction x , characterised as the loading (upsetting/compressing) direction, a strain range of $\varphi \approx 0.02$ to 1 was taken into account. Nevertheless, above the equivalent strain of $\varphi \approx 0.6$, steady stress states are expected, as is confirmed by the main yield stress curves in Fig. 2.

Furthermore, each time σ_{33} corresponds to x orthotropic axis, σ_{22} to y and σ_{11} to z .

For the calculation of σ_{11} , σ_{22} , σ_{33} and σ_{12} , σ_{23} , σ_{13} , which are assumed to be constants during the whole deformation process, the following procedures have been taken into account.

Generally, while general-use-obtained main yield and shear yield stresses have not been obtained at the same strain rates as occurred in the lab-scale study for determining anisotropic material flow listed in Table 1, linear interpolations between the main yield and shear yield stresses data (given as data arrays) at higher and lower strain rate were performed.

Procedures for calculation σ_{11} , σ_{22} , σ_{33} and σ_{12} , σ_{23} , σ_{13} .

1. For upsetting LD specimens, $\sigma_{11} = \sigma_{22}$, due to the cylindrical final shape, was considered as an average value of the main yield stresses in the TD direction from $\varphi \approx 0.02$ to $\varphi_{D_L} = \varphi_{D_T}$. Main stress σ_{33} was considered as an average value of the main yield stresses in the LD direction from $\varphi \approx 0.02$ to 1. Condition $\sigma_{12} = \sigma_{13}$ was considered as an average value of shear yield stresses in the TD direction from $\varphi \approx 0.02$ to φ_{D_T} while σ_{23} was considered as an average value of shear yield stresses in the LD direction from $\varphi \approx 0.02$ to 1.

2. For upsetting TD specimens, σ_{11} was considered as an average value of the main yield stresses in LD direction from $\varphi \approx 0.02$ to φ_{D_L} . Main stress σ_{22} was considered as an average value of the main yield stresses in the TD direction from $\varphi \approx 0.02$ to φ_{D_L} while σ_{33} was considered as an average value of the main yield stresses in the TD from $\varphi \approx 0.02$ to 1. Shear stress σ_{12} was considered as an average value of shear yield stresses in the TD direction from $\varphi \approx 0.02$ to 1, while σ_{13} was considered as an average value of shear yield stresses in the TD direction from $\varphi \approx 0.02$ to φ_{D_T} . Shear stress σ_{23} was considered as an average value of shear yield stresses in the LD direction from $\varphi \approx 0.02$ to φ_{D_L} .

3. For radial compressing of the TD specimens, σ_{11} was considered as an average value of the main yield stresses in the TD direction from $\varphi \approx 0.02$ to φ_{L_F} while σ_{22} was considered as an average value of the main yield stresses in the TD direction from $\varphi \approx 0.02$ to φ_{L_R} . Main stress σ_{33} was considered as an average value of the main yield stresses in the LD direction from $\varphi \approx 0.02$ to 1. Shear stress σ_{12} was considered as an average value of shear yield stresses in the TD direction from $\varphi \approx 0.02$ to φ_{L_F} while σ_{13} was considered as an average value of shear yield stress in the TD direction from $\varphi \approx 0.02$ to φ_{L_R} . Shear stress σ_{23} was considered as an average value of shear yield stresses in the LD direction from $\varphi \approx 0.02$ to 1.

4. For radial compressing of LD specimens, σ_{11} was considered as the maximal value of the main yield stresses in the LD direction. Main stress σ_{22} was considered as an average value of the main yield stress in the TD direction from $\varphi \approx 0.02$ to φ_{L_R} while σ_{33} was considered as an average value of the main yield stress in the TD direction from $\varphi \approx 0.02$ to 1. Shear stress σ_{12} was considered

as an average value of shear yield stresses in the TD direction from $\varphi \approx 0.02$ to 1 while σ_{13} was considered as an average value of shear yield stresses in the TD direction from $\varphi \approx 0.02$ to φ_{L_R} . Shear stress σ_{23} was considered as an average value of shear yield stresses in the LD direction from $\varphi \approx 0.02$ to φ_{L_F} .

Hill's anisotropic coefficients were calculated through Eqs. (5) and (6) afterwards, and are given in Table 2 beside determined values of σ_{11} , σ_{22} , σ_{33} , σ_{12} , σ_{23} and σ_{13} .

Table 2
Determined σ_{11} , σ_{22} , σ_{33} , σ_{12} , σ_{23} , σ_{13} in MPa and Hill's anisotropic coefficients

Upsetting LD: $\dot{\varphi} = 0.4 \text{ s}^{-1}$		
300°C	350°C	400°C
$\sigma_{11} = \sigma_{22} = 109.5$ $\sigma_{33} = 103.7$ $\sigma_{23} = 59.1$ $\sigma_{12} = \sigma_{13} = 53.1$	$\sigma_{11} = \sigma_{22} = 76.2$ $\sigma_{33} = 79.4$ $\sigma_{23} = 46.1$ $\sigma_{12} = \sigma_{13} = 41.4$	$\sigma_{11} = \sigma_{22} = 61.4$ $\sigma_{33} = 62.4$ $\sigma_{23} = 34.7$ $\sigma_{12} = \sigma_{13} = 33.8$
$F = 0.426$ $G = H = 0.538$ $L = 1.657$ $M = N = 2.05$	$F = 0.553$ $G = H = 0.474$ $L = 1.405$ $M = N = 1.742$	$F = 0.518$ $G = H = 0.490$ $L = 1.585$ $M = N = 1.674$
Upsetting LD: $\dot{\varphi} = 0.6 \text{ s}^{-1}$		
300°C	350°C	400°C
$\sigma_{11} = \sigma_{22} = 125.5$ $\sigma_{33} = 120.0$ $\sigma_{23} = 70.3$ $\sigma_{12} = \sigma_{13} = 62.1$	$\sigma_{11} = \sigma_{22} = 94.3$ $\sigma_{33} = 93.8$ $\sigma_{23} = 54.7$ $\sigma_{12} = \sigma_{13} = 48.8$	$\sigma_{11} = \sigma_{22} = 74.7$ $\sigma_{33} = 73.8$ $\sigma_{23} = 41.8$ $\sigma_{12} = \sigma_{13} = 41.1$
$F = 0.440$ $G = H = 0.531$ $L = 1.545$ $M = N = 1.981$	$F = 0.486$ $G = H = 0.506$ $L = 1.487$ $M = N = 1.866$	$F = 0.484$ $G = H = 0.507$ $L = 1.577$ $M = N = 1.625$
Upsetting TD: $\dot{\varphi} = 0.4 \text{ s}^{-1}$		
300°C	350°C	400°C
$\sigma_{11} = 134.7$ $\sigma_{22} = 104.5$ $\sigma_{33} = 100.6$ $\sigma_{23} = 41.3$ $\sigma_{12} = 58.0$ $\sigma_{13} = 61.1$	$\sigma_{11} = 94.3$ $\sigma_{22} = 74.7$ $\sigma_{33} = 73.5$ $\sigma_{23} = 38.1$ $\sigma_{12} = 42.6$ $\sigma_{13} = 44.7$	$\sigma_{11} = 69.3$ $\sigma_{22} = 61.0$ $\sigma_{33} = 60.5$ $\sigma_{23} = 31.5$ $\sigma_{12} = 33.8$ $\sigma_{13} = 35.2$
$F = 0.312$ $G = 0.407$ $H = 0.883$ $L = 3.818$ $M = 1.939$ $N = 1.747$	$F = 0.351$ $G = 0.393$ $H = 0.834$ $L = 2.279$ $M = 1.824$ $N = 1.654$	$F = 0.415$ $G = 0.431$ $H = 0.676$ $L = 2.052$ $M = 1.779$ $N = 1.640$
Upsetting TD: $\dot{\varphi} = 1.6 \text{ s}^{-1}$		
300°C	350°C	400°C
$\sigma_{11} = 158.3$ $\sigma_{22} = 121.4$ $\sigma_{33} = 117.2$ $\sigma_{23} = 48.5$ $\sigma_{12} = 66.8$ $\sigma_{13} = 72.5$	$\sigma_{11} = 113.3$ $\sigma_{22} = 91.9$ $\sigma_{33} = 89.9$ $\sigma_{23} = 42.4$ $\sigma_{12} = 51.0$ $\sigma_{13} = 54.7$	$\sigma_{11} = 84.5$ $\sigma_{22} = 73.6$ $\sigma_{33} = 73.0$ $\sigma_{23} = 35.5$ $\sigma_{12} = 41.1$ $\sigma_{13} = 43.5$
$F = 0.311$ $G = 0.400$	$F = 0.354$ $G = 0.407$	$F = 0.407$ $G = 0.427$

$H = 0.898$ $L = 3.789$ $M = 2.000$ $N = 1.695$	$H = 0.803$ $L = 2.714$ $M = 1.881$ $N = 1.631$	$H = 0.691$ $L = 2.358$ $M = 1.763$ $N = 1.574$
Radial compressing TD: $\dot{\varphi} = 0.6 \text{ s}^{-1}$		
300°C	350°C	400°C
$\sigma_{11} = 115.2$ $\sigma_{22} = 112.0$ $\sigma_{33} = 109.1$ $\sigma_{23} = 62.4$ $\sigma_{12} = 58.8$ $\sigma_{13} = 55.6$	$\sigma_{11} = 82.0$ $\sigma_{22} = 80.0$ $\sigma_{33} = 83.9$ $\sigma_{23} = 48.7$ $\sigma_{12} = 44.9$ $\sigma_{13} = 42.8$	$\sigma_{11} = 65.9$ $\sigma_{22} = 64.2$ $\sigma_{33} = 66.1$ $\sigma_{23} = 37.3$ $\sigma_{12} = 37.1$ $\sigma_{13} = 35.2$
$F = 0.446$ $G = 0.501$ $H = 0.555$ $L = 1.613$ $M = 1.817$ $N = 2.031$	$F = 0.546$ $G = 0.452$ $H = 0.502$ $L = 1.414$ $M = 1.661$ $N = 1.827$	$F = 0.515$ $G = 0.472$ $H = 0.512$ $L = 1.541$ $M = 1.554$ $N = 1.720$
Radial compressing TD: $\dot{\varphi} = 2.3 \text{ s}^{-1}$		
300°C	350°C	400°C
$\sigma_{11} = 132.4$ $\sigma_{22} = 130.5$ $\sigma_{33} = 125.4$ $\sigma_{23} = 71.6$ $\sigma_{12} = 63.3$ $\sigma_{13} = 62.5$	$\sigma_{11} = 101.7$ $\sigma_{22} = 98.6$ $\sigma_{33} = 99.1$ $\sigma_{23} = 55.8$ $\sigma_{12} = 51.0$ $\sigma_{13} = 48.3$	$\sigma_{11} = 79.5$ $\sigma_{22} = 77.0$ $\sigma_{33} = 77.9$ $\sigma_{23} = 42.8$ $\sigma_{12} = 42.8$ $\sigma_{13} = 40.3$
$F = 0.636$ $G = 0.519$ $H = 0.546$ $L = 1.633$ $M = 2.09$ $N = 2.140$	$F = 0.485$ $G = 0.477$ $H = 0.538$ $L = 1.596$ $M = 1.911$ $N = 2.134$	$F = 0.495$ $G = 0.471$ $H = 0.534$ $L = 1.667$ $M = 1.664$ $N = 1.881$
Radial compressing LD: $\dot{\varphi} = 0.6 \text{ s}^{-1}$		
300°C	350°C	400°C
$\sigma_{11} = 152.2$ $\sigma_{22} = 109.1$ $\sigma_{33} = 106.2$ $\sigma_{23} = 58.5$ $\sigma_{12} = 62.6$ $\sigma_{13} = 65.6$	$\sigma_{11} = 118.1$ $\sigma_{22} = 79.4$ $\sigma_{33} = 78.6$ $\sigma_{23} = 41.3$ $\sigma_{12} = 46.7$ $\sigma_{13} = 48.3$	$\sigma_{11} = 86.5$ $\sigma_{22} = 64.8$ $\sigma_{33} = 64.8$ $\sigma_{23} = 32.5$ $\sigma_{12} = 37.5$ $\sigma_{13} = 38.2$
$F = 0.296$ $G = 0.369$ $H = 1.000$ $L = 3.280$ $M = 1.972$ $N = 1.792$	$F = 0.301$ $G = 0.330$ $H = 1.095$ $L = 2.581$ $M = 2.016$ $N = 1.888$	$F = 0.352$ $G = 0.354$ $H = 0.907$ $L = 2.496$ $M = 1.874$ $N = 1.813$
Radial compressing LD: $\dot{\varphi} = 2.3 \text{ s}^{-1}$		
300°C	350°C	400°C
$\sigma_{11} = 185.7$ $\sigma_{22} = 125.8$ $\sigma_{33} = 122.5$ $\sigma_{23} = 52.7$ $\sigma_{12} = 69.1$ $\sigma_{13} = 73.8$	$\sigma_{11} = 139.5$ $\sigma_{22} = 97.1$ $\sigma_{33} = 95.6$ $\sigma_{23} = 43.1$ $\sigma_{12} = 53.8$ $\sigma_{13} = 56.1$	$\sigma_{11} = 104.9$ $\sigma_{22} = 77.1$ $\sigma_{33} = 76.7$ $\sigma_{23} = 35.6$ $\sigma_{12} = 43.8$ $\sigma_{13} = 44.7$
$F = 0.277$ $G = 0.353$ $H = 1.097$ $L = 3.915$ $M = 2.280$ $N = 1.998$	$F = 0.305$ $G = 0.346$ $H = 1.039$ $L = 3.412$ $M = 2.185$ $N = 2.012$	$F = 0.339$ $G = 0.351$ $H = 0.942$ $L = 2.999$ $M = 1.664$ $N = 1.881$

4.2. Description of determination the Hill's anisotropic coefficients for industrial-scale forging

The purpose of this study was also to analyse whether results obtained in the lab-scale study for determining anisotropic material flow can be used for the determining of Hills' anisotropic coefficient for forging slugs having bigger and different dimensions (diameter and length) at higher strain rates.

In fact, in industrial-scale forging, cylindrical slugs were forged in a radial direction using a screw press. This forging process can be considered in the same way as radial compressing of cylindrical specimens oriented in the LD direction; therefore, the same procedure as is described in the fourth paragraph of Chapter 4.1 was used for the determination of Hill's anisotropic coefficients.

Because it was expected that much higher strain rates would appear during industrial-scale forging and due to the observed major dependence of the main yield stresses on the strain rate, Hill's anisotropic coefficients were determined on the basis of the obtained main yield and shear yield stresses at the highest strain rate of $\dot{\varphi} = 10 \text{ s}^{-1}$.

Despite the unknown logarithmic deformation of φ_{L_R} and φ_{L_F} at $\dot{\varphi} = 10 \text{ s}^{-1}$, from the analysis of material flow at radial compressing of LD specimens in Table 1, it can be concluded that material flow has only minor influence on the strain rate. Therefore, the same value of φ_{L_R} and φ_{L_F} as was determined for radial compression of LD specimens at a strain rate of $\dot{\varphi} = 2.3 \text{ s}^{-1}$ and an initial temperature of the specimen of 300°C was used, i.e. the initial temperature of slugs used in industrial-scale forging trials was also 300°C . Hill's anisotropic coefficients are listed in Table 3.

Table 3

Determined σ_{11} , σ_{22} , σ_{33} , σ_{12} , σ_{23} , σ_{13} in MPa and Hill's anisotropic coefficients for industrial-scale forging

Radial forging cylindrical slug at: $\dot{\varphi} = 10 \text{ s}^{-1}$, $T=300^\circ\text{C}$	
$\sigma_{11} = 248.1$, $\sigma_{22} = 138.5$,	$F = 0.207$, $G = 0.326$,
$\sigma_{33} = 133.9$, $\sigma_{23} = 60.9$,	$H = 1.507$, $L = 4.435$,
$\sigma_{12} = 77.1$, $\sigma_{13} = 86.3$	$M = 2.762$, $N = 2.205$

5. FEM study

5.1. General data used for the definition of FEM models

FEM simulations were carried out in Deform 3D V10 software. For solving FEM computations, explicit Sparse solver and the conventional Newton-Raphson iteration method were used [12].

Plastic (anisotropic) characteristics of material (AZ80 alloy) was considered according to Hill's (1948) quadratic anisotropic yield law while mechanical properties during plastic deformation were defined according to general-use-obtained main yield stresses (flow curves) in the TD or LD orthotropic directions, which were inserted in the FEM model as data array.

Hill's anisotropic coefficients in FEM models were defined according to Table 2 for upsetting and compressing of small cylindrical specimens and Table 3 for forging of complicated industrial-scale part.

Other physical data of AZ80 alloy necessary for complete definition of the FEM model are represented in Table 4 [9]. The listed data were the same in all defined FEM models.

Table 4

Physical data of AZ80 alloy [9]

Density: 1740 kg/m^3
Young's modulus: 44.53 GPa
Poisson's ration. 0.358
Thermal expansion - function of temperature [$\text{mm}/^\circ\text{C}$]: 2.6407×10^{-5} at 250°C ; 2.5869×10^{-5} at 300°C ; 2.5279×10^{-5} at 350°C ; 2.4658×10^{-5} at 400°C
Thermal conductivity - function of temperature [$\text{J}/\text{m} \times \text{s} \times ^\circ\text{C}$]: 157 at 250°C ; 156 at 300°C ; 155 at 350°C ; 154 at 400°C
Specific heat: $1030 \text{ J}/(\text{kg} \times ^\circ\text{C})$
Emissivity ratio: 0.8
Environmental temperature: 25°C

All deformable specimens (objects) in the FEM models were 3D-meshed by the absolute number of tetrahedral elements having a minimal size of 1.4 mm and size ratio of 2, also kept during remeshing. During FEM computation and also during remeshing, target volume compensation has been taken into account to eliminate volume loss of deformable specimens. Deformable specimens were set as ideal plastic bodies while upper and lower dies (forging tool) were defined as rigid bodies having constant temperatures throughout the duration of the deformation process.

The temperature dependant Coulomb friction law was used for describing friction between the surface of deformable specimens and die's surface. Friction coefficients μ in Table 5 correspond to oil-based carbon lubricated forging of AZ80 alloy [13].

Table 5

Used Coulomb friction coefficients [13]

Temperature, $^\circ\text{C}$	250	300	350	420
Coefficient μ	0.05	0.08	0.10	0.14

5.2. FEM simulation results of lab-scale study for determining anisotropic material flow

In this part with FEM models, the same process parameters as used in the lab-scale study for determining anisotropic material flow were defined.

To summarise, TD- and LD-oriented specimens regarding the extrusion direction having dimensions of $\varnothing 16 \times 20 \text{ mm}$ were upset upright and compressed in the radial direction at three different initial temperatures (300°C , 350°C and 400°C) through constant ram speeds of 5 and 20 mm/s . To enable isothermal deformation, the defined tool temperature was the same as the initial temperature of specimens.

At the upsetting of LD and the radial compressing of TD specimens, the main yield stress data in the LD direction were used, while with all other FEM models the main yield stress data in the TD direction were used for describing mechanical properties during deformation, while Hill's anisotropic coefficients were defined accord-

ing to Table 2.

A comparison between 3D-digitalised real shapes and FEM computed 3D-shapes of compressed specimens is shown in Fig. 4.

Orientation		$v=5 \text{ mm/s}$			$v=20 \text{ mm/s}$		
		300 °C	350 °C	400 °C	300 °C	350 °C	400 °C
LD upsetting	Experiment						
	Simulation						
TD upsetting	Experiment						
	Simulation						
TD radial compression	Experiment						
	Simulation						
LD radial compression	Experiment						
	Simulation						

Fig. 4 Comparison of experimentally deformed and FEM computed specimens' footprints

From footprints of deformed specimens in Fig. 4, it is very clearly seen that the FEM simulation results suit lab-scale results very well, and also that determined Hill's anisotropic coefficients describe the anisotropic material characteristics in Hill's (1948) quadratic anisotropic yield law very well.

5.3. FEM simulation results of forging an industrial-scale part

In the second part of the FEM study, the forging of a complex industrial part (motorcycle handle bar) was simulated. In the FEM study, defined input process parameters corresponding to realistic process parameters, which were very carefully monitored during industrial-scale forging trials while material mechanical properties during plastic deformation were defined by the main yield stresses data in the TD direction and by Hill's anisotropic coefficients given in Table 3.

In the first forging operation, a slug having dimensions illustrated in Fig. 5, a was bent to a shape as shown on Fig. 5, b. In the FEM model, the bending operation was considered with an initial slug temperature of 300°C, constant ram speed of 10 mm/s and constant bending tool temperature of 25°C. Bending enables adapting the slug shape to the tool cavity (see Fig. 5, c).

In the second forging operation, the slug temperature was again defined at 300°C, because in industrial-scale forging the slug also was reheated back to 300°C.

The final shape of the motorcycle handle bar was forged in one stroke using 25% of maximal energy. In the FEM model screw press, the moment of inertia of 550000 Nms² and lead screw pitch of 43 mm/rev were defined by the available stroke energy of 11 MNm. The defined temperature of both upper and lower forging dies

having mirror symmetrical cavities was 120°C.

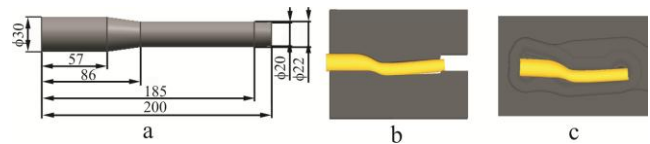


Fig. 5 a) Slug dimensions, b) bended slug and c) bended slug placed into the lower die cavity

In order to evaluate the accuracy of prediction of material flow with FEM models, comparisons of the 3D-digitalised shape and the FEM computed 3D-shape of industrial-scale forged parts have been performed. 3D-digitalisation was done with the ATOS II optical system. The comparison was made with special purpose software, GOM Inspect V7 SR2, through the best-fit method in which the shape of the FEM computed 3D-shape was compared to the referenced 3D-digitalised shape of the industrial-scale forged part.

In Fig. 6, a, the shape of the 3D-digitalised industrial-scale forged part is shown, while in Fig. 6, b the meshed FEM computed 3D-shape with colour-shaded temperature distribution is shown. In Fig. 6, c, differences between the 3D-digitalised shape and the FEM computed 3D-shape are analysed with colour-shaded technique.

From these results, it can be concluded that FEM simulation incorporating Hill's (1948) quadratic anisotropic yield law and determining Hill's anisotropic coefficients gives very reliable results with very small deviations from the real case. It must be also mentioned that in industrial-scale forged parts, flash cracking occurred, but that has not been taken into account in the FEM model. Cracking is certainly an additional reason for deviations between the 3D-digitalised shape and the FEM computed 3D-shape.

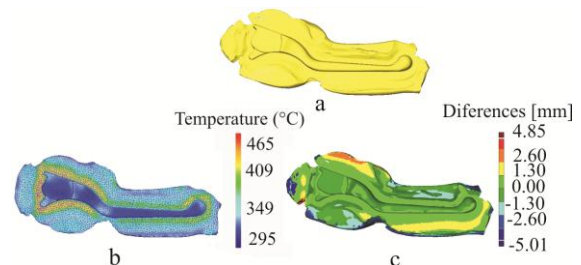


Fig. 6 Industrial-scale forged part a) 3D-digitalised and b) FEM simulated 3D-shape with temperature distribution and c) differences between 3D-digitalised and FEM computed 3D-shape

6. Conclusions

Despite simplifications in which material anisotropy was described by Hill's anisotropic coefficient defined as constants during entire plastic deformation, very good results concerning FEM prediction of anisotropic material flow using Hill's (1948) quadratic anisotropic yield law are observed.

It is also evident that anisotropic behaviour affects material flow during plastic deformation significantly with respect to loading direction or specimen placement.

On the basis of this study, procedures for determining Hill's anisotropic coefficients for other magnesium alloys can also be used. This approach can successfully be used in industrial practice.

Acknowledgements

A part of represented research work was performed within a Collective Research Project MagForge – Magnesium Forged Components for Structural Lightweight Transport Applications with Contract no.: COL-CT-2006-030208 founded by EC as a 6FP project.

References

1. **Hartley, P.; Pillinger, I.** 2006. Numerical simulation of the forging process, *Computer Methods In Applied Mechics And Engineering* 195: 6676-6690. <http://dx.doi.org/10.1016/j.cma.2005.03.013>.
2. **Yilmaz, N.F.; Eyercioglu, O.** 2008. Knowledge-based reverse engineering tool for near net shape axisymmetric forging die design, *Mechanika* 5(73): 65-73.
3. **Kurz, G.; Clauw, B.; Sillekens, W.H.; Letzig, D.** 2009. Die forging of the alloys AZ80 and ZK60, *TMS – Magnesium Technology* 197-202.
4. **Cazacu, O.; Plunkett, B.; Barlat, F.** 2006. Orthotropic yield criterion for hexagonal closed packed metals, *International Journal of Plasticity* 22: 1171-1194. <http://dx.doi.org/10.1016/j.ijplas.2005.06.001>.
5. **Kobold, D.; Pepelnjak, T.; Gantar, G.; Kuzman, K.** 2010. Analysis of deformation characteristics of magnesium AZ80 wrought alloy under hot conditions, *Journal of Mechanical Engineering* 12(56): 823-832.
6. **Wu, H.C.** 2003. On finite plastic deformation of anisotropic metallic materials, *International Journal of Plasticity* 19: 91-119. [http://dx.doi.org/10.1016/S0749-6419\(01\)00025-0](http://dx.doi.org/10.1016/S0749-6419(01)00025-0).
7. **Hill, R.** 1948. A theory of the yielding and plastic flow of anisotropic metals, *Proceedings of the Royal Society of London, The Royal Society*, 193(1033): 281-297.
8. **Rees, D.W.A.** 2006. *Basic engineering plasticity*, Elsevier, 339-367.
9. **Pepelnjak, T.; Popescu, G.**: Deliverable D2.5.1; Constitutive relationships and physical property data for modified feedstock. -www.magforge.eu.
10. **Lekhnitskii, S.G.** 1989. *Theory of Elasticity of an Anisotropic Body*. -Moscow – MIR Publishers, 15–78 (English translation of supplemented Russian edition from year 1977).
11. **Zilinskaite, A.; Ziliukas, A.** 2008. General deformation flow theory, *Mechanika* 2(70): 11-15.
12. *Deform 3D Version 6.1. -User's manual*. -Scientific Forming Technologies Corporation, 2009 (pdf format).
13. **Mannens, R.G.T.M.W.; Sillekens, H.** Deliverable D2.2.2; first generation of lubrication and tool-coating systems and their tribological characterisation. www.magforge.eu.

D. Kobold, G. Gantar, T. Pepelnjak

MAGNIO KALIOJO LYDINIO AZ80 ANIZOTROPINĖS ELGSENOS KARŠTOJO KALIMO METU ANALIZĖ BAIGTINIŲ ELEMENTŲ METODU

R e z i u m ė

Straipsnyje BEM imituojamas anizotropinis magnio AZ80 kaliojo lydinio tekėjimas karštojo tūrinio kalimo metu. Anizotropinės charakteristikos apibūdintos remiantis klasikiniu Hillo (1948) kvadratinio anizotropinio tekėjimo dėsnio. Nustatant realius BEM rodiklius, įgalinančius per priimtina skaičiavimo laiką kompleksiskai imituoti tūrinio formavimo operaciją, pasiūlytas supaprastintas būdas Hillo anizotropijos koeficientams nustatyti naudojant juos kaip konstantą. Pateikti laboratorinėmis ir gamybinėmis sąlygomis, naudojantis Hillo anizotropijos koeficientais ir mechaninėmis savybėmis BEM atliktų tyrimų rezultatai. Šie rezultatai palyginti su eksperimentiniais tyrimais. Parodyta, kad pasiūlytasis metodas gali būti sėkmingai taikomas gamyboje.

D. Kobold, G. Gantar, T. Pepelnjak

FINITE ELEMENT ANALYSES OF MAGNESIUM AZ80 WROUGHT ALLOY ANISOTROPIC BEHAVIOUR DURING WARM FORGING

S u m m a r y

This paper deals with the FEM simulations of anisotropic flow during bulk forming (forging) of magnesium AZ80 wrought alloy at warm conditions. Anisotropic characteristics are described by the classical formulation of Hill's (1948) quadratic anisotropic yield law. To define reliable FEM models capable of carrying out numerical simulations of complex bulk forming operations in a reasonable amount of computing time, a simplified approach for determining Hill's anisotropic coefficients as constants is proposed. On the basis of the determined Hill's anisotropic coefficients and the mechanical properties, the results of an extensive FEM study of lab-scale and industrial-scale forging are shown. FEM results are also compared to the actual obtained results. It is shown that the approach presented can be successfully used in industrial practice.

Keywords: Magnesium forging, anisotropy, Hill's law, FEM.

Received April 15, 2011

Accepted May 30, 2012